AIChE

Mixing in Tangentially Crossing Microchannels

Denz Lee and Yu Tzu Chen
Institute of Aeronautics and Astronautics, National Cheng Kung University, Tainan, Taiwan, Republic of China

DOI 10.1002/aic.12299
Published online June 22, 2010 in Wiley Online Library (wileyonlinelibrary.com).

In this study, we have demonstrated that effective mixing can be achieved in simple and regular crossing channels. The dynamical processes combining split-and-recombine and chaotic mixing elements of stretching and folding were discussed. In channels with simple turns (up/down/right/left), flow could be stretched; on the other hand, tangential crossings could yield folding. Theoretically, repeating stretching and folding then result in the increase of interfacial area and decrease of striation thickness which facilitate the eventual mixing by diffusion. Practically, the structural sequence of turning and/or crossing affects the performance of the mixing. Three types of micromixers were studied, and the simulated performance was favorably compared with the published data. Experiments were carried out to qualitatively demonstrate the typical performance in the mixers.
 AIChE J, 57: 571–580, 2011
Keywords: micromixer, crossing channel, chaotic mixing

Introduction

Micromixer has found its wide application in many areas ranging from Micro ElectroMechanical Systems (MEMS) to micro total analysis systems (μTAS), microreactors, biochips, and others.[1] In the category of passive mixing, various principles and devices have been proposed, among them, hydrodynamic focusing,[2] split-and-recombine (SAR),[3] lamination,[4] and chaotic advection[5,6] are most frequently mentioned. Other interesting studies include mixing of viscoelastic fluids,[7] multivortex micromixing,[8] mixing by using polymer additives[9] among others. Further review on micromixers is referred to Hardt et al.,[10] Hessel et al.,[11] and Nguyen and Wu.[4] One of the features of micromixing is in its relatively slow, laminar flow condition usually at the Reynolds numbers of the order of 1. Mixing eventually counts on diffusion to complete, the key is then how to make diffusion effective by increasing the interface and reducing the diffusion distance.

Chaotic advection has been used in many mixers, macro, and micro. The term of "chaotic advection" was first introduced in 1982,[12,13] and the concepts of chaotic mixing were discussed in details in Ottino's book.[14] Wiggins and Ottino[15] focused on mathematical foundation of chaotic mixing and suggested the conditions for the best quality mixing. The baker's transformation was taken as the centerpiece for describing the dynamical framework. The concepts have also been extended to micromixing by Ottino and Wiggins.[16] The study suggested that the key to effective mixing lies in creating stretching and folding, and a necessary condition for chaos is the crossing of two successive streamline portraits at the moving direction when superimposed and projected onto the cross sectional plane. Other discussions are also found in Karniadakis et al.[17] Chaotic advection in passive micromixers provides an attractive mechanism for achieving efficient mixing in biofluidic arena in which limiting the strain on an embedded macromolecule is desirable.

Following the concepts, various geometries have been devised to facilitate chaotic mixing. Structured grooves enhancing mixing has been studied by Stroock et al.,[5,6] Wang et al.,[18] and Yang et al.,[19] respectively. In the category of lamination, SAR mixing could yield very thin lamellae in a few steps and avoid unmixed islands.[10] Kim et al.[20] combined SAR and chaotic advection in their serpentine mixer and claimed that a high level of efficient mixing was achieved. Earlier, Liu et al.[21] studied the serpentine mixer and quantified the performance by the light intensity of the images. Recently, Tung et al.[22] investigated the mixing details inside a droplet moving through a serpentine

Correspondence concerning this article should be addressed to D. Lee at denzlee@mail.ncku.edu.tw.

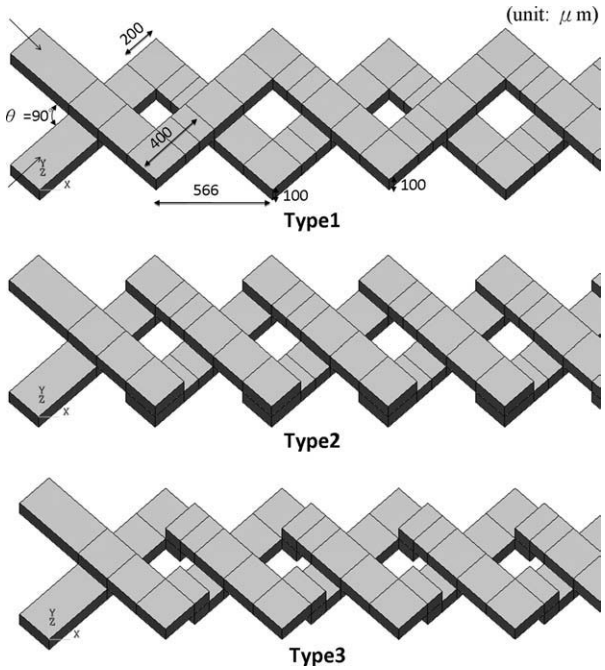

Figure 1. Configuration of the three types of the micromixers.

micromixer. Interesting photos and mechanisms explaining the chaotic mixing are demonstrated.

To characterize the performance of the mixers, the Lyapunov exponents (λ) and Poincaré sections were mathematically elucidated by Ottino[14] and Wiggins and Ottino.[15] λ is the long time average of the stretching rate, when the largest λ of a dynamic system is positive, the system is chaotic.[23] Studies are also seen in Niu and Lee,[24] Xia et al.[25] and Park and Kwon[26] among others. Poincaré section converts the flow into a map, this allows a systematic reduction in complexity of problems by means of a reduction in the number of dimensions. In application, the mapping "compresses" a 3D flow field into a 2D cross sectional one, and a 3D particle path will turn into a planar trace map. On the tools to quantify the mixing, particle tracking simulation has been used, for example, by Aubin et al.,[27] Kang and Kwon,[28] and Xia et al.[25]

Micromixer is a useful component in μTAS and biochips, the requirements of less driving force, easy fabrication, and limitation of the fluid strain on the sample give rise to the use of mixers in less complicate configuration. Simple crosses have been used by Wang et al.,[29,30] with patterned groove the mixers claimed to have achieved the performance over the existing herringbone mixers. Ismagilov et al.[31] and Lee et al.[32] studied the flows in tangentially crossing microchannels and reported that the movement of the fluid in this simple geometry demonstrates the feature of controllable flow split ratio upon crossing. This earlier study[32] prompted the idea of constructing simple and regular configuration mixers, which work on the mechanisms of folding and stretching[14] by flow crossing. By connecting multiple crosses, the flow can be repeatedly split and recombined. With up/down steps at the turning of the channels, chaotic advection can be generated. The combination of the two mechanisms in repeating crossing channels may yield satisfactory mixing. In this study, the performance of this mixer was evaluated with the particle tracing techniques. The Poincaré section and Lyapunov exponent were used to characterize the mixers. The results were compared with those in the literature. Experiments for the qualitative validation of the mixing were conducted. The roles of turning and crossing were discussed, and the guidelines for the geometry design were suggested.

Methods

Geometrical configuration strongly influences the performance of a mixer. In this study, three types of mixers which are based on 3D crossing structures studied previously[32] were tested. The configuration of these mixers is given in Figure 1. The channels were of the width (w) of 200 μm and height (h) of 100 μm, i.e., the aspect ratio, AR ($= h/w$) is 0.5, and the fraction of flow turning to the other channel upon crossing, would be about 0.45 at the Reynolds number (Re) of 0.1 according to the previous study.[32] Type1 is featured with simple two-layer crossings, each channel remains in the same level with periodical crossing to the other channel in the other level. In Type2 and Type3 mixers, the channels run through both layers alternatively. The difference between the two types is whether the channels turn vertically (up/down) first (Type2) or horizontally (right/left) first (Type3) at the corners. The sequence of turning may influence the effectiveness of the stretching and folding.

Numerical aspects

The simulation was carried out by using the commercial computer program CFD-ACE+ (CFD Research Corporation). The equations solved were the 3D Navier-Stokes equations and the species convection–diffusion equations. Structured grid was used for the simulation. Grid tests were conducted and described in the previous study.[32] The fair grid size in a 200 (w) $\times$ 100 (h) channel was 5 $\times$ 5 $\times$ 5 (in μm) for the width, length, and height, respectively. This amounts to about 64,000 grids in the junction alone and the total number of grid was about one million. If necessary, zonal or adaptive gridding methods which locally enhance the grid density developed by the authors[33,34] can be considered for better resolution. Performance comparison of all types of mixers in this study was based on the simulation with the same grid size. The spatial discretization was conducted by using the second-order upwind scheme, and the conjugate-gradient solver for velocity iteration and multigrid method for pressure correction. The convergence criteria were set at 10^{-4}.

In this study, to characterize our 3D time-independent spatial periodic mixers, particle tracking,[25,27,28] Poincaré section, Lyapunov exponent (λ), and its mapping (λ-map)[14,15] have been used. Particle dispersion studies provide intuitive information in understanding the mixing operation. Poincaré sections are used to identify the chaotic regions. Lyapunov exponent (λ) and λ-map can be used to quantify the chaotic strength and to evaluate the chaotic behavior of the mixer.

Using particle tracking method, the distribution profiles of the particles in Poincaré section will reflect the mixing process. In particular, uniform dispersion of particles that are initially confined in a blob can be utilized to characterize

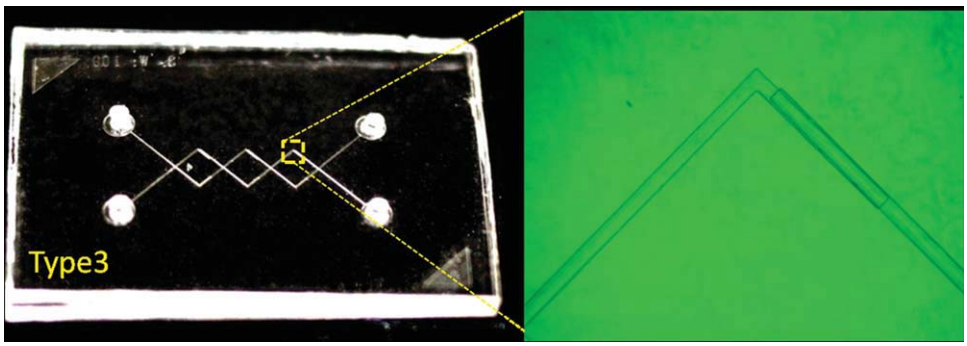

Figure 2. Finished product of the 3D crossing microchannel Type3.

[Color figure can be viewed in the online issue, which is available at wileyonlinelibrary.com.]

mixing. In this study, the Poincaré section was obtained by collecting every intersection of the passive particle trajectories at each marked crossing section for about 500 periods of mixing unit, and projected onto a single map. Quantification of chaotic strength, on the other hand, can be achieved by calculating the finite time Lyapunov exponent (λ).[25] The Lyapunov exponent (λ) represents the average exponential rate of stretching of two initially neighboring particle trajectories and can be calculated as

$$\lambda = \lim_{N\to\infty} \frac{1}{N} \sum_{i=1}^{N} \ln\left(\frac{\delta^{N+1}(x)}{\delta^{N}(x)}\right) \tag{1}$$

where $\delta(x)$ is the distance of the fluid trajectories, which is a function of the mixer length x. N represents the Nth mixer unit. λ is calculated within fixed crossing units for convenient comparison of various micromixers.. Positive λ exhibits a chaotic behavior, whereas zero λ represents a stable property. By plotting the λ-map, the mixing behavior of a specific mixer can be revealed. The mixer flow fields can be overall chaotic, there also can be isolated regions which persistently maintain unmixed.

In addition to the Lagrangian approach, practically, mixing efficiency quantification using numerical solutions of the species transport equation can also be useful. The mixing index α can be defined as[35]:

$$\alpha = 1 - \sqrt{\frac{\sigma^2}{{\sigma_{\max}}^2}} = 1 - \frac{\sigma}{0.5} \tag{2}$$

$$\sigma\sqrt{\frac{1}{N}\sum_{i=1}^{N}(C_i - \overline{C})^2} \tag{3}$$

σ is the root mean square deviation of the concentration at the interested plane, N is the number of grid points in the cross section, C_i is the concentration value at the ith grid, and $\overline{C}$ is the concentration of complete mixing. The initial concentration at the inlet which is either 0 or 1.0, and $\sigma_{\max}$ is the maximum variance of the mixture (unmixed). In this problem, $\sigma_{\max} = 0.5$ and a perfect mix would reach $\overline{C} = 0.5$ also. A

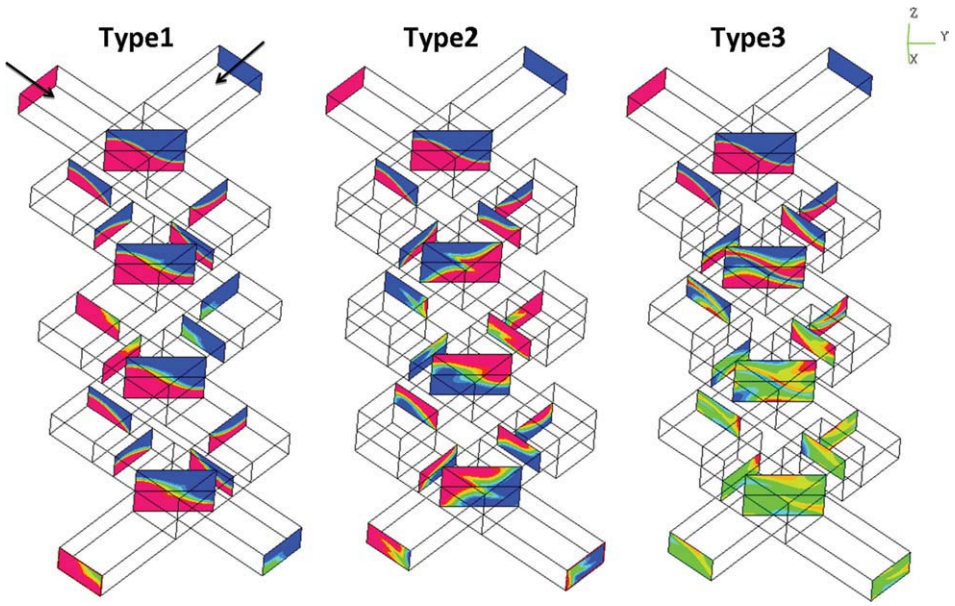

Figure 3. Comparison of the progress of mixing at the four crossings in three types of mixers.

AR = 0.5, $Re = 0.1$, $D = 4 \times 10^{-9}$ m^2 s^{-1}. [Color figure can be viewed in the online issue, which is available at wileyonlinelibrary.com.]

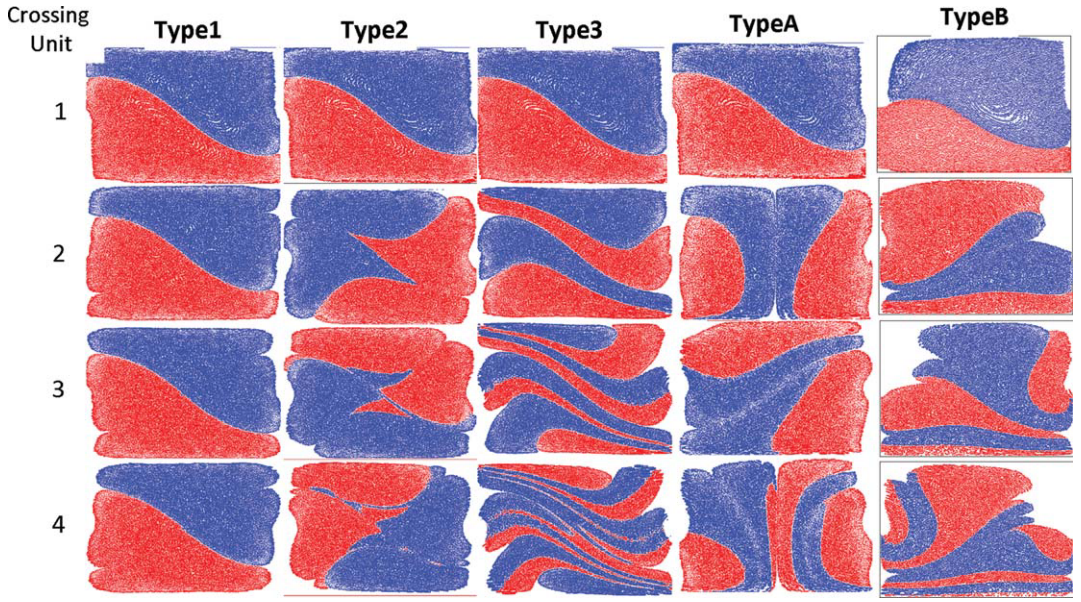

Figure 4. The color particles distribution at four successive crossings of the five different types of mixers.

AR = 0.5, *Re* = 0.1. [Color figure can be viewed in the online issue, which is available at wileyonlinelibrary.com.]

smaller deviation signifies better mixing and α ranges from 0 for no mixing to 1 for perfect mixing.

Experimental aspects

To facilitate the measurement of the light intensity at the crossings, with the main features kept, the dimension of the actual mixers for the experiments was modified to 100 μm × 50 μm (AR = 0.5) for the width and height. The length between the turnings and the crossings was extended to ease the alignment and measurement. This variation was also applied to all the reference mixers for the comparison. The dimension used in the corresponding simulation was modified accordingly. The 3D microfluidic devices were fabricated in two poly(dimethylsiloxane) (PDMS). Because the fabrication process with PDMS is well known, the details will not be repeated here. Briefly, the SU-8 photoresist was developed in a SU-8 developer solution and was hard baked on a hot plate to finish the patterned master mold. The degassed PDMS mixture was then poured onto the patterned master mold and cured. Next, on the cured replicas, the inlet and outlet holes were drilled. Subsequently, the two distinguishable PDMS slabs (one for the upper channel and the other the lower channel) were treated by oxygen plasma and aligned and pressed together in DI water carefully. Finally, the microfluidic device

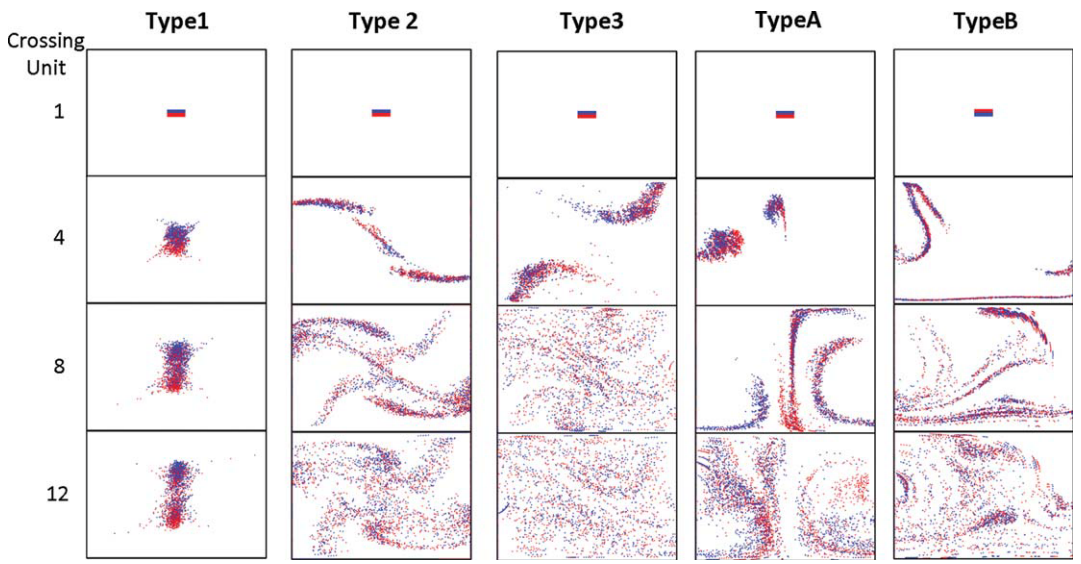

Figure 5. The blob tests in the five mixers.

AR = 0.5, *Re* = 0.1. [Color figure can be viewed in the online issue, which is available at wileyonlinelibrary.com.]

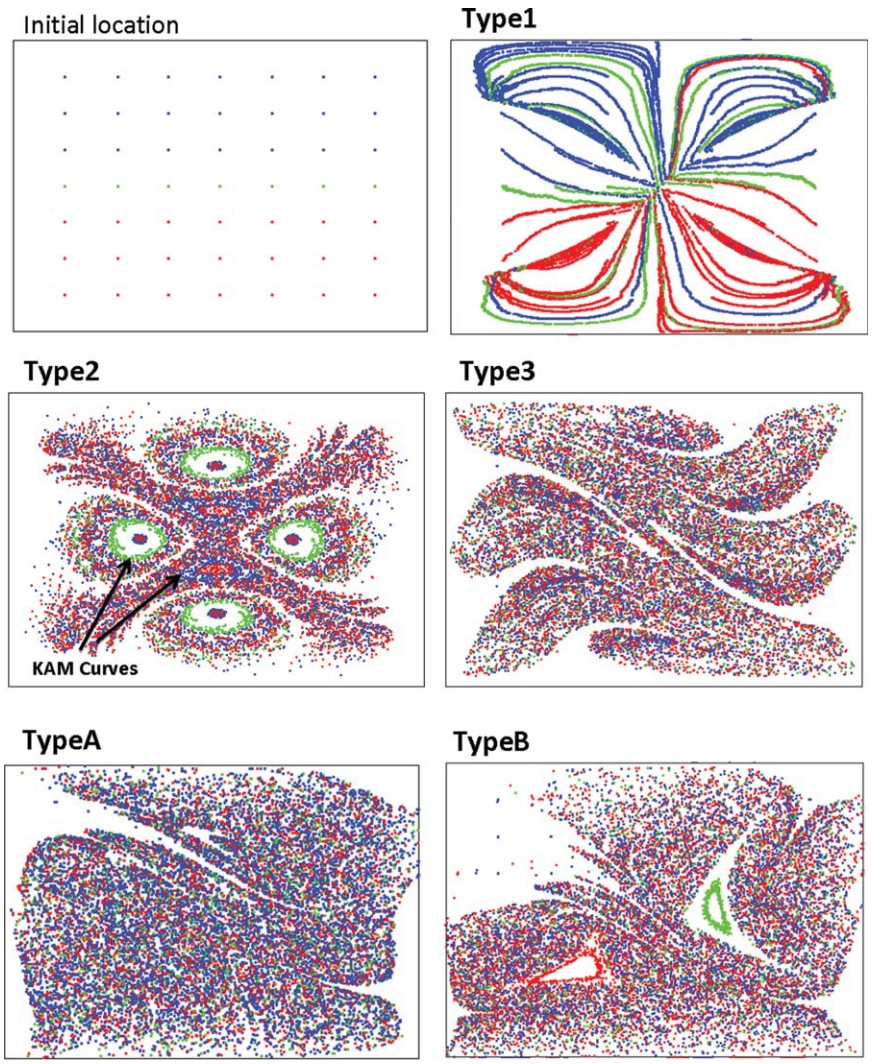

Figure 6. Poincaré sections for the five mixers.

AR = 0.5, Re = 0.1. [Color figure can be viewed in the online issue, which is available at wileyonlinelibrary.com.]

was baked. Details and relevant concerns can be found in the reference by the authors.[36] Figure 2 displays the finished microchannels for the experiments.

The basic experimental setup was similar to that in the previous study.[32] The image was captured by 7-megapixel camcorder equipped with an inverted fluorescence microscope (IX-71, Olympus, with 10× objective lens NA = 0.25, $\pm d \sim$ 18.4 μm). Mixing in the microchannel is commonly evaluated by observing color or light intensity variations of a dye or pH indicator.[21,37] Two approaches were used here, first, dilution of Rhodamine 6G fluorescent dye (concentration of 0.052 mM) with deionized water. Second, diluted black ink (25%) with deionized water. Images of the mixture are captured through a Nikon SMZ800 microscope at 50 times magnification with a CCD camera (TGCD-9648I, Telgen).

Before the experiments, the linear relationship has been verified between the normalized intensity and the concentration used in the microchannel. The pictures were first transferred into a gray-scale image that contained 0–255 intensity levels. Then, the intensity of each pixel along the detection line (the diagonal line of the crossing zone) was normalized with the background value as

$$I_n^* = \frac{I_n - I_B}{I_F - I_B} \tag{4}$$

where I_n^* is the normalize intensity along the detection line, I_n is the intensity in the pixel n, and I_B and I_F is the background and flooded intensity (that of the channel filled with fluorescent dye) of each sampled image, respectively. Therefore, the intensity level of each pixel was rescaled to a value between 0 and 1. The intensity profiles (to represent normalized concentration) along the detection lines of the cross section could be obtained.

Results and Discussion

In this section, general flow features and the mixing performance in the three types of mixers will be presented and discussed. Then the mixing performance will be compared

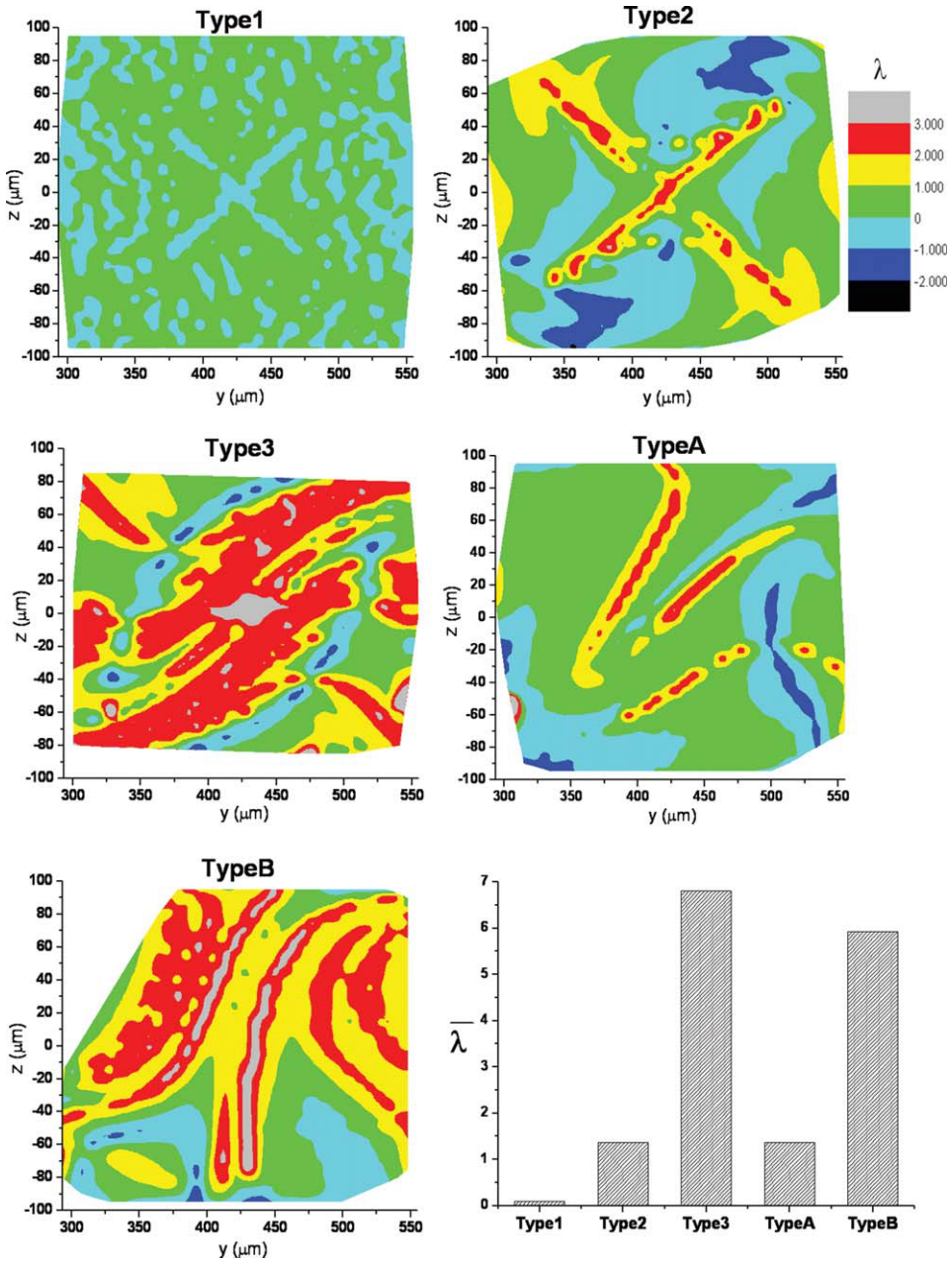

Figure 7. The λ-map of each mixer and the comparison of the average λ of the five mixers.

AR = 0.5, Re = 0.1. [Color figure can be viewed in the online issue, which is available at wileyonlinelibrary.com.]

with the published literature. Unless specified otherwise, all the simulations are in AR = 0.5, Re = 0.1, and the Peclet number is 2.5×10^5 with the diffusivity D considering the mixture of 1-μm latex beads in water is 4×10^{-13} m^2 s^{-1}. In the calculations, this smaller D can also signify the effect of chaotic mixing rather than that by diffusion.

Flow patterns

In Figure 3, the progress of mixing within the four crossings in three types of mixers is shown. In Type1 mixer, obviously the flow pattern regularly recovers every other crossing with this type of geometry. In this pattern, the flows recombine at the cross cannot result in the folding needed for mixing. With Type2 mixer, channel flows run between the two layers alternatively. The flow pattern, although better, recovers also every other crossing except that the two streams swapped. Folding at the crossing is not successful either. In Type3 mixer, the flows turn first then go to the other layer. Note also the geometry change at the turning corners. It is seen that upon the recombination at the second crossing, due to the reorientation of the two parts of each stream (observe the difference of the "blue" stream before the second crossing between Type2 and Type3), the crossing successfully "folds" and doubles the number of striations, and consequently, reduce their thickness and diffusion time between lamellae. The improvement of mixing can be spied at the exit.

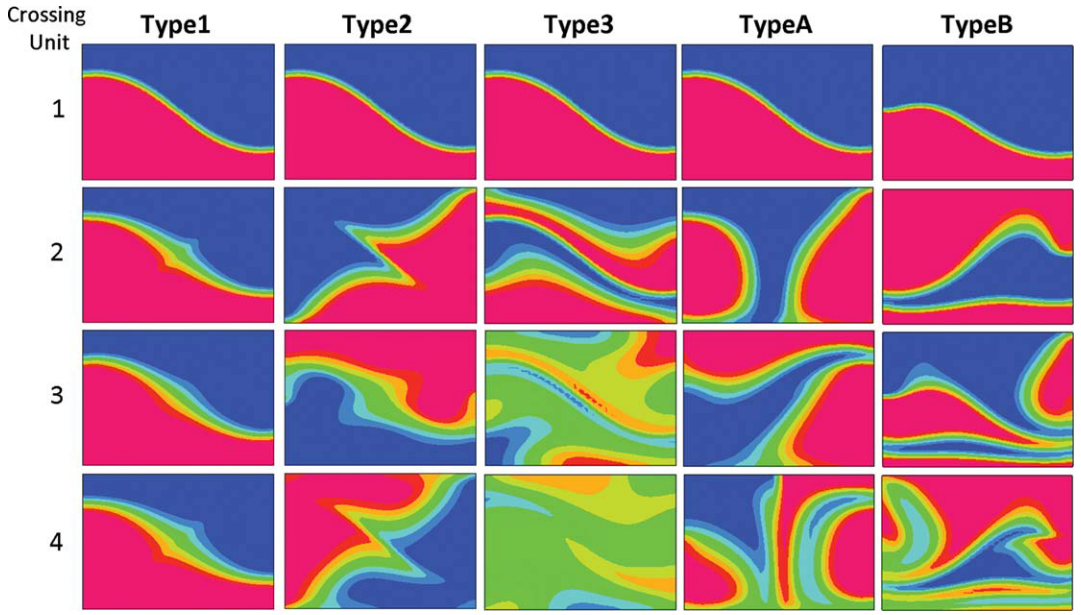

Figure 8. The simulated concentration contours at the four crossing sections.

AR = 0.5, Re = 0.1. [Color figure can be viewed in the online issue, which is available at wileyonlinelibrary.com.]

The observation reveals that when the flow turns and switches (ascends/descends) to the other layer, it matters how the turns and switches are arranged. Here, in Type2, the flow completes its descent and then turns at the corner, the flow changes direction two times. In Type3, the flow turns first, followed by a descent, the flow changes direction thrice. The difference of the flow orientation can be seen before the second crossing (Figure 3). The distribution of the two streams after the turn in Type3 favors more obvious folding than that in Type2. In general, frequent switch between the two layers favors the mixing at the expense of pressure drop. The channel layer structure clearly plays significant role on SAR mixing.

Next, we compare these mixers with the similar ones proposed in other study.[25,38] With the same flow conditions, all three types of the mixers together with TypeA and TypeB mixers in the literature[38] (model A and B in their Figure 1) were simulated with CFD-ACE+. Using particle tracking, Figure 4 shows the cross sectional color particle distribution at four successive crossings of all the five mixers. When comparing with the other mixers, Type3 clearly demonstrates well organized and repeating folding upon crossing. However, this function is not intrinsic; rather, it closely correlates with the upstream flow/structure conditions. Among others, TypeB mixer also exhibits its folding function, and the striation is thicker and less regular though.

Mixing performance

A further test using two blobs of 3000 colored particles each was conducted. The blobs were placed in the center of the first crossing, initially, and allowed to flow downstream through multiple crossings with flow SAR. In Figure 5, observing the last cross unit, Type3 demonstrates again the most uniform mixing among all. Poincaré sections for various mixers are then shown in Figure 6. The analysis has used initially 49 particles for 500 periods. In these figures, the dotted areas indicate the areas of the existence of chaotic behavior, whereas the areas of circles (islands) and lines as appear in Type1, Type2, and TypeB denote nonchaotic behavior. Typical KAM (Kolmogorov-Arnold-Moser) curves[14] are shown in Type2 which separate the chaotic and nonchaotic areas, the particles inside the curves will remain inside and thus preventing chaotic mixing from happening inside. Both Type3 and TypeA demonstrate well-chaotic flow without "islands" of ill-mixing regions. Figure 7 displays the λ-maps within four crossing units in the five mixers. Type1 is seen to be a stable system, its λ values are very close to zero, Type2 and TypeA are relatively better. Type3 and TypeB are in the best. High λ value implies high-stretching rate and better mixing. Figure 7 also shows the average λ of each of the five mixers and Type3 has the largest value and the most desirable chaotic behavior. To further "visualize" the mixing, the numerical solution of species transport equations were also calculated to provide the concentration contours. The two streams are in blue and red, respectively. Figure 8 presents the concentration contours at the four crossing sections. Type3 mixer shows the least unmixed region at the last section, implying the most uniform overall mixing.

Another quantifiable indication of mixing is the mixing index aforementioned. Figure 9a exhibits the mixing index of each mixer at the fourth crossing. For Reynolds number below 10, Type3 mixer outperforms the rest. Interestingly, the performance of Type3 drops quickly when the Reynolds number is greater than 10. The reasons maybe are as follows, first, increasing inertial effect due to higher flow rate changes the relative importance of the basic mixing mechanisms of Type3. Type3 mixer takes advantages of both mechanisms of SAR and the chaotic mixing, when Re increases the flow profile changes, the effectiveness of folding due to SAR decreases quickly as demonstrated in Figure 9b for Re = 100. Besides, it was also seen that isolated core flow in the stream is formed due to the stronger secondary flows

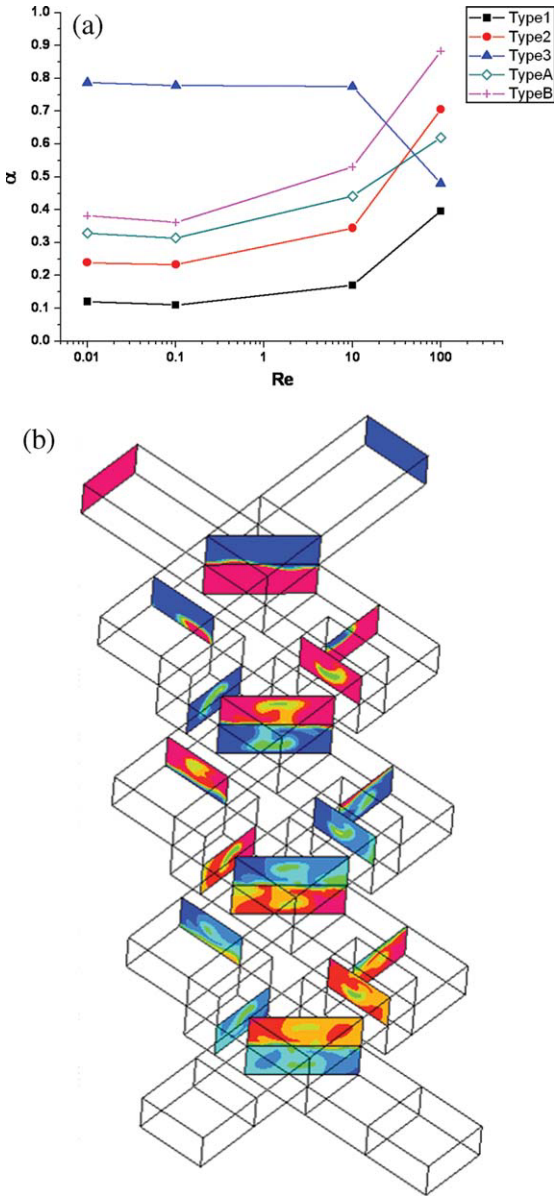

Figure 9. (a) The effect of flow rate/*Re* on mixing index of each mixer. (b) The flow profile of Type3 at high Reynolds number, *Re* = 100.

AR = 0.5, $D = 4 \times 10^{-13}$ m^2 s^{-1}. [Color figure can be viewed in the online issue, which is available at wileyonlinelibrary.com.]

caused by the turns. The persistent unmixed core can be seen clearly in most of the cross sections for *Re* at about 50 and higher. Even the chaotic mixing may be enhanced due to higher flow rate, it may not compensate the loss due to the weakening lamination from SAR. This would not happen to the other types of mixers, which basically less rely on the regular folding in the crossings. According to the previous study,[32] at AR = 0.5, as *Re* increases the flow split ratio drops, for example, from about 0.5 at *Re* = 1 to about 0.1 at *Re* = 100. This unequal flow split ratio at the crossings (see Figure 9b after the first crossing) further hampers the even mixing of the two streams. Nevertheless, Type3 demonstrates a consistent performance for flow below *Re* = 10, this may find application in situations of small volume sample. Note that if needed the channels still can be adjusted with smaller aspect ratio AR to retrieve equal split ratio at crossings.[32] For example, at *Re* = 50, AR = 0.3 can be used to yield the split ratio of about 0.5. For lower *Re* (<10), better performance points to the mixers with AR near 0.5 (for 1:1 split).

Experimental tests

Experiments on the various types of mixers with the same flow conditions have been conducted to further qualify the general performance of the mixers. For visualization, dilute black ink and fluorescence dye were used as aforementioned. Simulation was also carried out to contrast the experimental results. Note that the diffusivity here for the solutions is chosen as 2.8×10^{-11} m^2 s^{-1}. The simulated concentration profiles at the first 4 crossings in Type3 mixer are shown in Figure 10a cross sectional view, Figure 10b overall view. Note that the values in all depth are superimposed for the overall view. Figures 10c, d display the optical view near the crossings. Careful contrast of the light intensity between the inlets of the first and the exits of the last crossing reveals the progress of mixing, and it is better observed in fluorescent dye.

To facilitate further comparison, these optical images were quantified by using the methods mentioned earlier. The distribution of the normalized light intensity I_n^* from the measurements and the calculated concentration from the simulations are plotted across the normalized channel width W^* in Figure 11 for comparison. Note that the value of I_n^* as well as the average concentration will both approach 0.5 when uniform mixing is achieved. The figure shows the values at the first crossing and the results of mixing after four crossings, and both Type3 mixer and TypeA mixer[38] are demonstrated. The blue and cyan lines are the simulated concentration distribution at the first and fourth crossing, respectively. The black and red lines are the experimental ones at the first and fourth crossing, respectively.

The results showed that in Type3 mixer, after four crossings high degree of uniformity is achieved experimentally and numerically. The detailed calculation revealed that this uniformity was attained gradually from the inlet crossing to the exit. In these tests, with the similar size and flow condition at *Re* = 0.1, Type3 was seen to outperform the other mixer after four crossings.

The experimental data curves are not as sharp as the simulation ones, the discrepancies can be attributed to a few facts. First, the simulations were based on the ideal geometry of the channels, on the other hand, channel fabrication, limited by the current facilities and techniques, and generally would not yield the "exact" shape (e.g., round corners are expected). Consequently, the flow field would not be exactly the same. Second, the detection facilities and the method had their limits and errors as well. For example, along the detection line (at the crossing), the light intensity was measured across the depth of two layers, the image was not as sharp. Near the edges of the channels, light intensity could be distorted by the wall. Third, unstable pumping and light sources could be annoying too. Exact measurements would be difficult; nevertheless, qualitative trends are agreeable as seen.

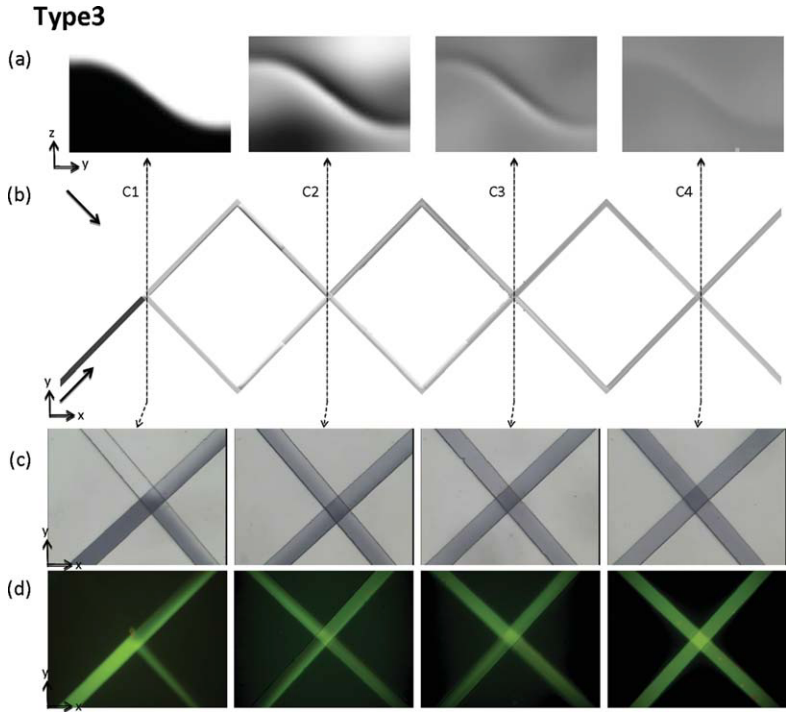

Figure 10. The simulated concentration distribution in (a) cross sections and (b) overall view, and the experimental observation using (c) black ink and (d) fluorescent dye.

AR = 0.5, $Re = 0.1$, $D = 2.8 \times 10^{-10}$ m^2 s^{-1} (Rhodamine 6G).

[Color figure can be viewed in the online issue, which is available at wileyonlinelibrary.com.]

Summary

In this study, we have demonstrated that a novel high-performance mixer can be obtained by using the simple and regular design, easy fabrication tangential crossings. The study tried to rationalize the performance based on the mechanisms of SAR and chaotic advection. In most of the mixing indicators, this Type3 mixer demonstrates the best performance. The mixer is well suitable for the Reynolds number below 10 when the mechanism of SAR can take effective role in folding. Arrangement of the geometrical factors such as AR, turnings, and crossings is obviously important and useful in the design of the mixer. Albeit simple, periodical crossings together with regularly alternating turns can yield high performance in mixing. Design rules are hinted in the study.

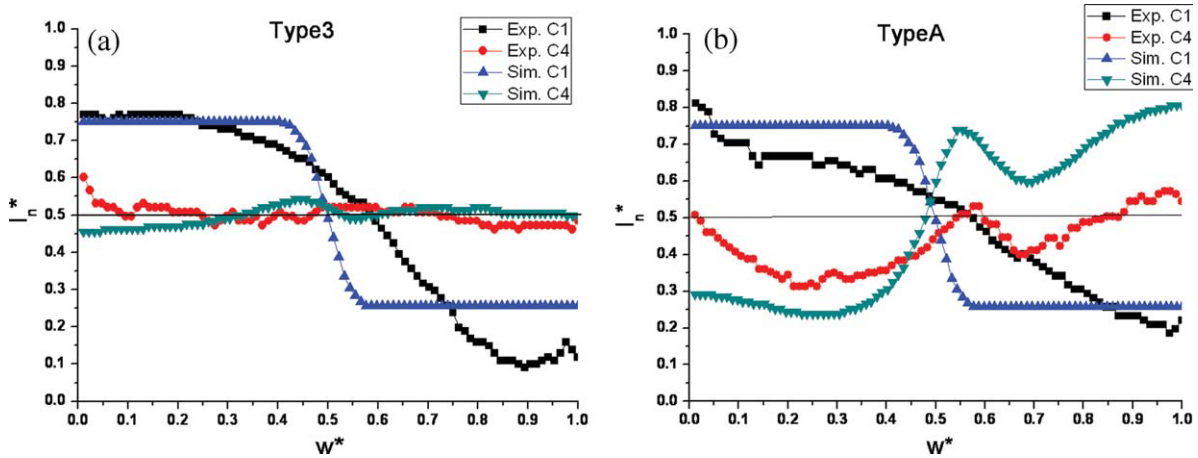

Figure 11. Distribution of the normalized light intensity and the simulated concentration across the section width *W at the first (C1) and the fourth crossing (C4) in the (a) Type3 mixer and (b) TypeA mixer.[38]**

AR = 0.5, $Re = 0.1$, $D = 2.8 \times 10^{-10}$ m^2 s^{-1}. [Color figure can be viewed in the online issue, which is available at wileyonlinelibrary.com.]

Acknowledgments

This study was partially sponsored by the National Science Council of Taiwan under the project NSC 96-2221-E-006-299.

Literature Cited

1. Demello AJ. Control and detection of chemical reactions in microfluidic systems. *Nature*. 2006;442:394–402.
2. Hessel V, Hardt S, Lowe H, Schönfeld F. Laminar mixing in different interdigital micromixers: I. Experimental characterization. *AIChE J*. 2003;49:566–577.
3. Schönfeld F, Hessel V, Hoffmann C. An optimized split-and recombine micro mixer with uniform chaotic mixing. *Lab Chip*. 2004;4: 65–69.
4. Nguyen NT, Wu Z. Micromixers—a review. *J Micromech Microeng*. 2005;15:R1–R16.
5. Stroock AD, Dertinger SKW, Ajdari A, Mezic I, Stone HA, Whitesides GM. Chaotic mixer for microchannels. *Science*. 2002;295: 647–651.
6. Stroock AD, Dertinger SKW, Whitesides GM, Ajdari A. Patterning flows using grooved surfaces. *Anal Chem.* 2002;74:5306–5312.
7. Gan HY, Lam YC, Nguyen NT, Tam KC, Yang C. Efficient mixing of viscoelastic fluids in a microchannel at low Reynolds number. *Microfluid Nanofluidics*. 2007;3:101–108.
8. Sudarsan AP, Ugaz VM. Multivortex micromixing. *Proc Natl Acad Sci USA*. 2006;103:7228–7233.
9. Groisman A, Steinburg V. Efficient mixing at low Reynolds numbers using polymer additives. *Nature*. 2001;410:905–908.
10. Hardt S, Drese KS, Hessel V, Schönfeld F. Passive micromixers for application in the microreactor and μTas fields. *Microfluid Nanofluidics*. 2005;1:108–118.
11. Hessel V, Lowe H, Schönfeld F. Micromixers—a review on passive and active mixing principles. *Chem Eng Sci*. 2005;60:2479–2501.
12. Aref H. Stirring by chaotic advection. *J Fluid Mech*. 1984;143:1–21.
13. Aref H. The development of chaotic advection. *Phys Fluids*. 2002; 14:1315–1325.
14. Ottino JM. *The Kinematics of Mixing:Stretching, Chaos, and Transport*. Cambridge: Cambridge University Press, 1989.
15. Wiggins S, Ottino J. Foundations of chaotic mixing. *Philos Trans R Soc Lond A*. 2004;362:937–970.
16. Ottino JM, Wiggins S. Introduction: mixing in microfluidics. *Philos Trans R Soc Lond A*. 2004;362:923–935.
17. Karniadakis G, Beskok A, Aluru N. *Microflows and Nanoflows*. New York: Springer, 2005.
18. Wang H, Iovenitti P, Harvey E, Masood S. Numerical investigation of mixing in microchannels with patterned grooves. *J Micromech Microeng*. 2003;13:801–808.
19. Yang JT, Huang KJ, Lin YC. Geometric effects on fluid mixing in passive grooved micromixers. *Lab Chip*. 2005;5:1140–1147.
20. Kim DS, Lee SH, Kwon TH, Ahn CH. A serpentine laminating micromixer combining splitting/recombination and advection. *Lab Chip*. 2005;5:739–747.
21. Liu RH, Stremler MA, Sharp KV, Olsen MG, Santiago JG, Adian RJ, Aref H, Beebe DJ. Passive mixing in a three-dimensional serpentine microchannel. *J Microelectromech Syst*. 2000;9:190–197.
22. Tung KY, Li CC, Yang JT. Mixing and hydrodynamic analysis of a droplet in a planar serpentine micromixer. *Microfluid Nanofluidics*. 2009;7:545–557.
23. Lee YK. Lyapunov exponents of a micro chaotic mixer. *Int J Nonlinear Sci Numer Simul*. 2002;3:561–564.
24. Niu X, Lee YK. Efficient spatial-temporal chaotic mixing in microchannels. *J Micromech Microeng*. 2003;13:454–462.
25. Xia HM, Shu C, Wan SYM, Chew YT. Influence of the Reynolds number on chaotic mixing in a spatially periodic micromixer and its characterization using dynamical system techniques. *J Micromech Microeng*. 2006;16:53–61.
26. Park JM, Kwon TH. Numerical Characterization of three-dimensional serpentine micromixers. *AIChE J*. 2008;54:1999–2008.
27. Aubin J, Fletcher DF, Bertrand J, Xuereb C. Characterization of the mixing quality in micromixers. *Chem Eng Technol*. 2003;26:1262–1270.
28. Kang TG, Kwon TH. Colored particle tracking method for mixing analysis of chaotic micromixers. *J Micromech Microeng*. 2004;14: 891–899.
29. Wang L, Yang JT. An overlapping crisscross micromixer using chaotic mixing principles. *J Micromech Microeng*. 2006;16:2684–2691.
30. Wang L, Yang JT, Lyu PC. An overlapping crisscross micromixer. *Chem Eng Sci*. 2007;62:711–720.
31. Ismagilov RF, Rosmarin D, Kenis PJA, Chiu DT, Zhang W, Stone HA, Whitesides GM. Pressure-driven laminar flow in tangential microchannels: an elastomeric microfluidic switch. *Anal Chem.* 2001;73:4682–4687.
32. Lee D, Chen YT, Bai TY. A study of flows in tangentially crossing micro-channels. *Microfluid Nanofluidics*. 2009;7:169–179.
33. Lee D, Tsuei YM. A hybrid adaptive gridding procedure for the recirculating fluid flow problem. *J Comput Phys*. 1993;108:122–141.
34. Lee D, Chen JY. Numerical simulation of flow fields in a tube with two branches. *J Biomech*. 2000;33:1305–1312.
35. Engler M, Kockmann N, Kiefer T, Woiias P. Numerical and experimental investigations on liquid mixing in static micromixers. *Chem Eng J*. 2004;101:315–322.
36. Chen YT, Lee D. A bonding technique using hydrophilic SU-8. *J Micromech Microeng*. 2007;17:1978–1984.
37. Munson MS, Yager P. Simple quantitative optical method for monitoring the extent of mixing applied to a novel microfluidic mixer. *Anal Chim Acta*. 2004;507:63–71.
38. Xia HM, Wan SYM, Shu C, Chew YT. Chaotic micromixers using two-layer crossing channels to exhibit fast mixing at low Reynolds number. *Lab Chip*. 2005;5:748–755.

Manuscript received Sept. 18, 2009, revision received Mar. 1, 2010, and final revision received May 18, 2010.